



# Distinguishing nitrogen-containing sites in SiO<sub>2</sub>/4H-SiC(0001) after nitric oxide annealing by X-ray absorption spectroscopy

Noritake Isomura,\* Katsuhiko Kutsuki, Keita Kataoka, Yukihiro Watanabe and Yasuji Kimoto

Received 5 November 2018

Accepted 26 January 2019

Toyota Central R&D Laboratories Inc., 41-1 Yokomichi, Nagakute, Aichi 480-1192, Japan.

\*Correspondence e-mail: isomura@mosk.tytlabs.co.jp

Edited by S. M. Heald, Argonne National Laboratory, USA

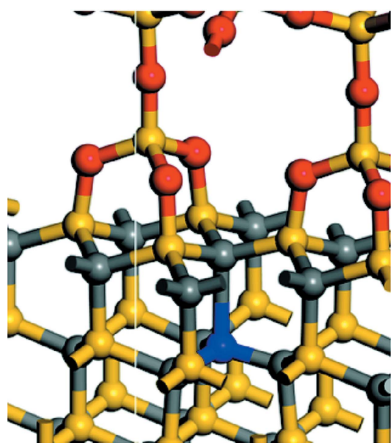
**Keywords:** X-ray absorption spectroscopy; XAS; X-ray absorption fine structure; XAFS; SiC–MOS; interface structure.

The atomic structure of nitrogen at the SiO<sub>2</sub>/4H-SiC(0001) interface has been investigated using X-ray absorption spectroscopy (XAS) in two nitric oxide annealed samples, one of which was oxidized in dry O<sub>2</sub> (NO-POA) prior to the experiment. The peak shapes and energies of the observed and simulated spectra are in agreement and indicate that the N-containing sites could be the substitutional C site at the interface for the NO-annealed sample and the interstitial site in the interior of SiC for the NO-POA-annealed sample. XAS analysis distinguished between the N-containing sites at the SiO<sub>2</sub>/SiC interface.

## 1. Introduction

Semiconductor devices manufactured using silicon carbide (SiC) can be operated at higher breakdown voltages, switching speeds and temperatures than those exhibited by devices that are manufactured using only silicon (Okumura, 2006; Kimoto, 2015). SiC metal-oxide semiconductor field-effect transistors (MOSFETs) are expected to be used in next-generation vehicles such as electric and fuel-cell vehicles (Shen & Omura, 2007). The performance, especially channel mobility, of SiC MOSFETs is limited by defects at the SiO<sub>2</sub>/SiC interface. The introduction of interfacial nitrogen by annealing in nitric oxide reduces the interface state density (Li *et al.*, 1997; Chung *et al.*, 2000; Yoshioka *et al.*, 2012). The states of interfacial N have been investigated (Kosugi *et al.*, 2011; Xu *et al.*, 2014); however, the atomic structure about N after NO annealing in substitutional and interstitial sites is not well understood even though this can result in differences in interface defects.

Kosugi *et al.* (2011) reported that N atoms were present as nitrides in the SiC interior when annealed at 800–1467°C under 20% NO (Ar balance). Xu *et al.* (2014) reported that N was directly incorporated into SiC or the first layers of SiC when annealed at 1175°C in NO after oxidation in dry O<sub>2</sub>. The local environment of interfacial N and its chemical state were investigated and observed to be identical regardless of the annealing conditions (oxidation by dry O<sub>2</sub> or not). Both studies used X-ray photoelectron spectroscopy (XPS), which is sensitive to the chemical state but not to the atomic structure (Briggs & Rivière, 1983). Hence, it is difficult to distinguish between the substitutionally and interstitially incorporated N, with a few exceptions, *e.g.* N-doped TiO<sub>2</sub> (Palgrave *et al.*, 2009). In contrast to substitutional N that only bonds to Ti, interstitial N may bond to Ti and O. The latter is highly electronegative, resulting in a large chemical shift that



can be detected by XPS. Shirasawa *et al.* (2007) used low-energy electron diffraction (LEED) and a scanning tunneling microscope (STM) and reported a silicon oxynitride layer with a heterodouble-layer structure; a silicate monolayer on a silicon nitride monolayer with Si–O–Si bridge bonds was formed by annealing in N<sub>2</sub> with residual oxygen. Therefore, the location of N atoms could not be determined at least for the case of NO annealing. Additionally, LEED and STM can be used for the thin layer formed at the surface. However, they could not be applied for an interface with an overlayer such as the SiO<sub>2</sub>/SiC interface, since they are relatively surface-sensitive methods.

In this study, we used X-ray absorption spectroscopy (XAS) to analyze the N incorporated into the SiO<sub>2</sub>/4H-SiC(0001) interface after NO annealing. The X-ray absorption near-edge structure (XANES) spectra obtained by XAS vary according to the local atomic structure around the target element, even without long-range periodicity (Norman, 1986). The atomic structures can be distinguished by comparison with standard spectra obtained theoretically (Mizoguchi *et al.*, 2009, 2012). In the theoretical calculations, the SiO<sub>2</sub>/SiC interface is modeled, which is different from a similar study by Hamada *et al.* (2017) who used a simple bulk model. The substitutionally incorporated N is defined as N changing place with Si, C or O, or as N filling an Si, C or O vacancy, in SiC and SiO<sub>2</sub>. The interstitially incorporated N is defined as N in the lattice of SiC or SiO<sub>2</sub>, and its actual position is determined by a geometrical optimization in the calculation.

## 2. Experimental and theoretical methods

The experimental observations were conducted at the soft X-ray absorption spectroscopy beamline, BL12, of the SAGA Light Source (SAGA-LS) (Kaneyasu *et al.*, 2009), which has an electron storage ring with a 75.6 m circumference and is operated at 1.4 GeV and 300 mA. Quasi-monochromatic X-rays ranging in energy from 40 eV to 1500 eV were produced using a varied-line-spacing plane grating. The energy resolution ( $E/\Delta E$ ) was approximately 2500 at 400 eV. The X-ray beam from the beamline was normal to the sample surface, and the beam spot dimensions were 1.5 mm (horizontal) × 0.6 mm (vertical). In the total electron yield (TEY) XAS measurements, the drain current ( $I$ ) of the samples was detected (Isomura *et al.*, 2015);  $I$  was normalized by the incident X-ray intensity, which was determined using the drain current ( $I_0$ ) of an Au mesh placed between the final mirror and the sample. The base pressure of the main chamber was approximately  $3 \times 10^{-8}$  Pa.

We prepared two different N-containing SiO<sub>2</sub>/SiC samples for interface analysis with TEY-XAS. The 4H-SiC(0001) Si-face substrates were annealed in a ramp-heating furnace. One was annealed at 1300°C for 30 min in 10% NO (N<sub>2</sub> balance) (hereafter NO-ox). The SiO<sub>2</sub> film was grown to a thickness of 6 nm. The other was annealed at 1300°C for 7 min in 100% oxygen (SiO<sub>2</sub> film thickness: 10 nm) and was then annealed under the same conditions as NO-ox (1300°C, 30 min, 10% NO) (hereafter NO-POA for nitric oxide post-oxidation

annealing). In both samples, the SiO<sub>2</sub> films were thinned to the same thickness (~3 nm), within the probing depth (1–10 nm) of the TEY-XAS (Cook *et al.*, 2009), in a 1% aqueous hydrogen fluoride solution (etching rate: 4–8 nm min<sup>-1</sup>). A thick (>100 nm) silicon nitride film was also used for comparison (hereafter Si–N).

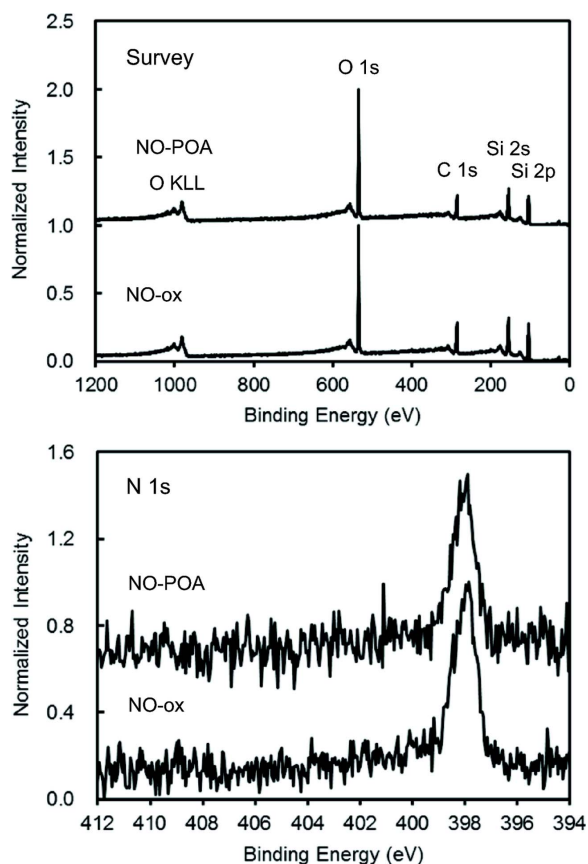
Prior to the XAS measurements, chemical states of N were investigated for the N-containing SiO<sub>2</sub>/SiC samples by conventional XPS. XPS measurements were performed using PHI-5500 with a hemispherical energy analyzer and a monochromated X-ray source (Al K $\alpha$ , 1486.6 eV). The emission angle of analyzed electrons was set to 0° (normal to the surface). The pass energies were 117.4 eV and 11.75 eV for the survey and core level spectra, respectively.

To distinguish between the N-containing sites, the SiO<sub>2</sub>/SiC interface was modeled by inserting N atoms into the lattice. A combination of  $\beta$ -tridymite SiO<sub>2</sub> and 4H-SiC (Si-face), with the smallest mismatch of lattice constant among the various polymorphs of SiO<sub>2</sub> (Ono & Saito, 2015), was used as the initial structure in the calculations. A slab model was also used in which the thicknesses of the SiO<sub>2</sub>, SiC and vacuum layers were 10 Å, 10 Å and 15 Å, respectively. The SiC layer contained five Si–C bilayers, and the bottom two layers were constrained in their bulk positions. The total number of Si, O and C atoms in each unit cell was 138. The dangling bonds on the vacuum-layer sides were terminated by hydrogen. Geometrical optimizations and XANES spectra simulations were performed via density-functional calculations using the CASTEP plane-wave code (Clark *et al.*, 2005), aided by the Materials Studio software (BIOVIA). Ultrasoft pseudopotentials and the generalized gradient approximation were used in the calculations (Perdew, 1985). In the XANES calculations, the ultrasoft pseudopotentials were generated on-the-fly (Gao *et al.*, 2009), where one core electron was eliminated from the 1s core level in the core-hole calculations. The calculation ‘Quality’ in the geometrical optimizations was set to ‘Fine’ (energy tolerance: 10<sup>-5</sup> eV per atom; maximum displacement tolerance: 10<sup>-3</sup> Å; cutoff energy: 340 eV). The calculation ‘Quality’ in the XANES spectra simulations was also set to ‘Fine’ (cutoff energy: 550 eV). To make the computational XANES comparable with the experimental results, the energy was broadened with an instrumental smearing of 1.0 eV. In the pseudopotential method, the transition energy cannot be evaluated. It was derived from the total energy difference between the excited and ground states, following the procedure by Mizoguchi *et al.* (2009).

## 3. Results and discussion

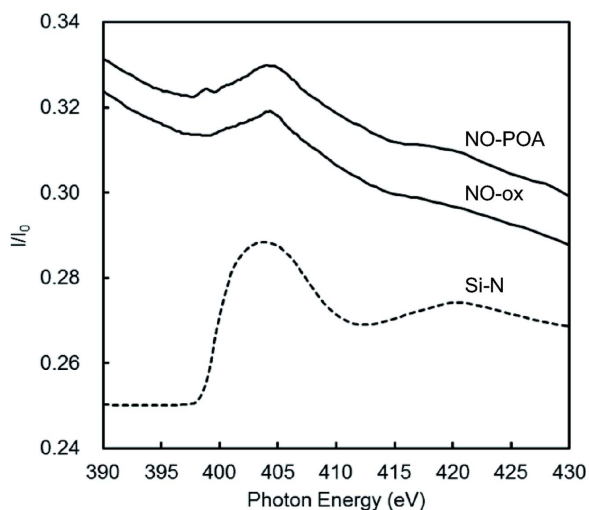
Fig. 1 depicts the XPS spectra for the N-containing SiO<sub>2</sub>/SiC samples (NO-ox and NO-POA). Photoelectron and Auger peaks are observed and are assigned to Si, O, C and N contained in the samples. In the N 1s spectra, single peaks can be seen at 398.0 eV, which are assigned to nitrides because of the agreement with the result reported by Kosugi *et al.* (2011).

Fig. 2 depicts the N K-edge XANES spectra for the N-containing SiO<sub>2</sub>/SiC samples (NO-ox and NO-POA) along



**Figure 1**  
XPS spectra for the N-containing SiC samples annealed in NO ambient.

with that for Si–N. The spectra for NO-ox and NO-POA exhibit small N *K*-edge peaks on a strong downward sloping background with energy. The background is attributed to the C *K*-edge peak in SiC that exists at low energy (generally at ~285 eV). Si–N shows a main peak at 404.0 eV, which agrees with the peak energy of  $\alpha$ -Si<sub>3</sub>N<sub>4</sub> (Chang *et al.*, 1998). The NO-



**Figure 2**  
N *K*-edge XANES spectra for N-containing SiO<sub>2</sub>/SiC samples annealed in NO ambient and NO-POA along with that for the Si–N film sample (bottom). For Si–N, the intensity (*I*/*I*<sub>0</sub>) is smaller and the background is constant at 0.22.

ox sample has a sharp-topped peak at 404.0 eV, that is, the same energy as Si–N. Conversely, the NO-POA sample exhibits a broad peak at 404.5 eV and a small pre-edge peak at 399.0 eV, *i.e.* an energy difference of 5.5 eV. In both samples (NO-ox and NO-POA), the peak energies nearly agree with Si–N, suggesting the presence of Si–N bonds. The spectral features of the NO-ox and NO-POA samples are compared with that of the standard theoretically obtained spectra.

Fig. 3 depicts the geometrically optimized interface structures of  $\beta$ -tridymite SiO<sub>2</sub>/4H-SiC (Si-face) with N incorporated at various substitutional and interstitial sites near the interface. The substitutional C sites at the interface and in the SiC interior are depicted in Figs. 3(*a*) and 3(*b*), respectively. Interstitial N sites bonded to C and two Si atoms at the SiC and SiO<sub>2</sub> sides are depicted in Figs. 3(*c*) and 3(*d*), respectively.

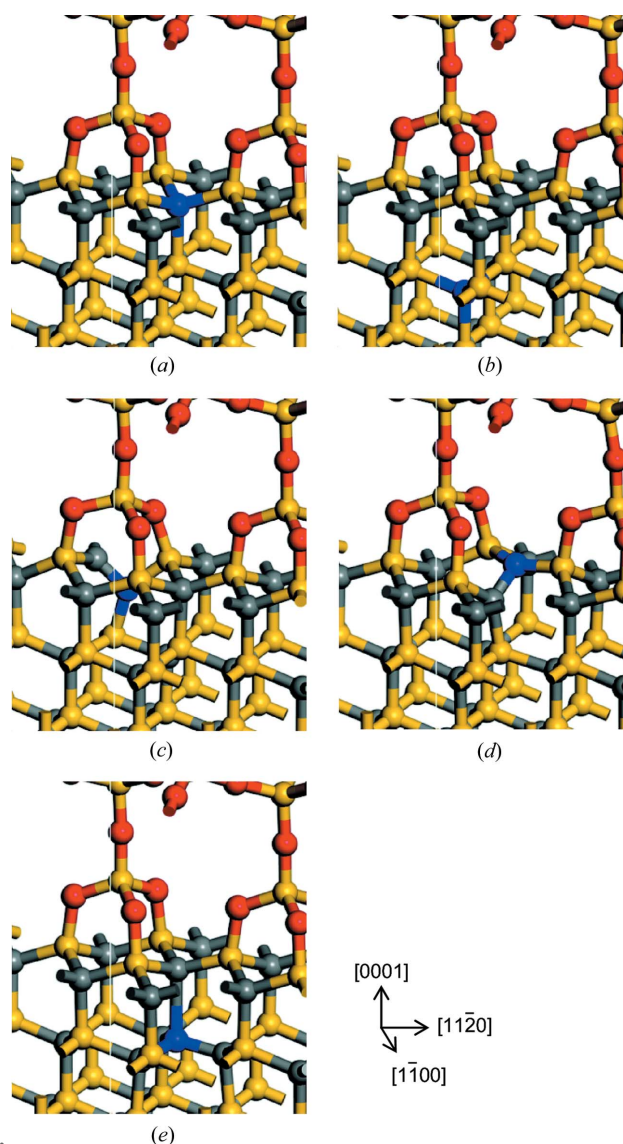


**Figure 3**  
Geometrically optimized interface structures of  $\beta$ -tridymite SiO<sub>2</sub>/4H-SiC (Si-face) with nitrogen: (*a*) substitutional C site at the interface and (*b*) at the SiC interior; (*c*) interstitial sites at the SiC and (*d*) at the SiO<sub>2</sub> side; (*e*) substitutional Si site at the SiC interior. Yellow, gray, red and blue denote the Si, C, O and N atoms, respectively. The crystal orientation for SiC is also depicted.

The substitutional Si site at the SiC interior is shown in Fig. 3(e). Although other structures were modeled, the geometrical optimization of the models with a substitutional Si site at the interface and a substitutional O site in the SiO<sub>2</sub> interior did not converge, and their figures are not depicted.

Fig. 4 depicts the simulated N *K*-edge XANES spectra for the N incorporated in the SiO<sub>2</sub>/SiC interface [Figs. 3(a)–3(e)] along with that for bulk  $\alpha$ -Si<sub>3</sub>N<sub>4</sub>. For comparison, the measured spectra for N-containing SiO<sub>2</sub>/SiC samples were normalized after the backgrounds were subtracted by a general method for XAS analysis using the *ATHENA* data processing suite package (Ravel & Newville, 2005), and are also depicted in Fig. 4. In the simulated spectra, the  $\alpha$ -Si<sub>3</sub>N<sub>4</sub> has a peak at 410.0 eV, located higher in energy by 6.0 eV than

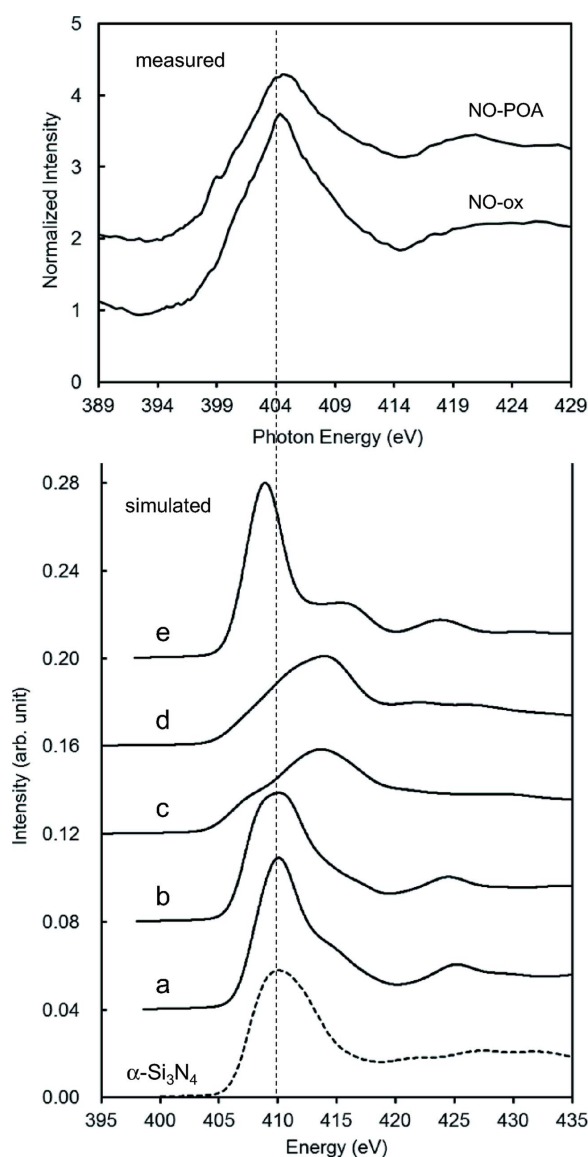


**Figure 4**  
The simulated N *K*-edge XANES spectra for N incorporated at the SiO<sub>2</sub>/SiC interface [in Fig. 3(a)–3(e)] along with that of bulk  $\alpha$ -Si<sub>3</sub>N<sub>4</sub> (bottom). For comparison, the measured spectra for N-containing SiO<sub>2</sub>/SiC samples are also depicted. The measured spectra were normalized after the backgrounds were subtracted, and were shifted in energy with reference to silicon nitride.

the peak corresponding to the Si–N film. Mizoguchi *et al.* studied the XANES spectra simulated using *CASTEP* in detail. They reported that the transition energy was overestimated by approximately 1% relative to the absolute energy (Mizoguchi *et al.*, 2012), which is a similar trend in other calculations (Mizoguchi *et al.*, 2004, 2008; Tanaka *et al.*, 2005), although the spectral shape was consistent with the experiment (Mizoguchi *et al.*, 2009). Ikeno & Mizoguchi (2017) reported that the overestimation may stem from an underestimation of the electronic correlation because of the restriction to electronic configurations (Slater determinants) and the insufficient treatment of core-hole screening effects. The aforementioned high energy of 6.0 eV is close to the overestimated value of 4.1 eV (1% of 410.0 eV), suggesting systematic errors in the *CASTEP* calculations. Therefore, the measured spectra are compared with the simulated spectra in ‘relative energy’ with reference to silicon nitride (Si–N and  $\alpha$ -Si<sub>3</sub>N<sub>4</sub>, respectively).

The substitutional C site at the interface [Fig. 4(a)] exhibits a sharp-topped peak at the same energy as  $\alpha$ -Si<sub>3</sub>N<sub>4</sub> (410.0 eV), which is consistent with NO-ox in peak shape and relative energy. Although the substitutional C site in the SiC interior [Fig. 4(b)] exhibits a peak at the same energy as that in Fig. 4(a), the peak-top shape is broad. Furthermore, the substitutional Si site in the SiC interior [Fig. 4(e)] exhibits a sharp-topped peak similar to that exhibited by Fig. 4(a), and a clear shoulder is present at 416.0 eV. Thus, the spectra for both sites [Figs. 4(b) and 4(e)] suggest different features for the NO-ox sample. It is suggested that the N-containing site in the case of NO-ox is the substitutional C site at the interface [Fig. 3(a)], showing the spectrum of Fig. 4(a).

The interstitial site, with an asymmetrical structure around N, in the SiC side [Fig. 4(c)] exhibits a broad-topped peak at 413.5 eV and a small pre-edge peak (like a shoulder) at 408.0 eV, indicating an energy difference of 5.5 eV. The XANES spectra are also sensitive to symmetry which can lead to pre-edge (Tanaka *et al.*, 1988), causing the pre-edge peak, *e.g.* N interstitial sites in bulk SiC in the calculated XANES spectra (Hamada *et al.*, 2017). In Fig. 4(c), the peak shape with the pre-edge peak resembles that in the NO-POA sample, and the energy difference (5.5 eV) between the main and pre-edge peaks agrees with the NO-POA sample, although the relative energy is higher by 3.0 eV. Hamada *et al.* (2017) reported that the calculated XANES spectra for interstitial N in SiC exhibited a main peak at higher energy than that of Si<sub>3</sub>N<sub>4</sub> (Hamada *et al.*, 2017), in agreement with the simulations in this study. In the N-containing sites in the NO-POA sample, the interstitial sites in the SiC side [Fig. 3(c)], showing the spectrum of Fig. 4(c), are least dominant. This is because it cannot be determined whether the spectrum with the broad-top peak includes other spectra and whether these spectra are small.

#### 4. Conclusions

The atomic structures of N incorporated in the SiO<sub>2</sub>/SiC interface after NO annealing were investigated by XAS. Two

NO-annealed 4H-SiC(Si-face) samples were used, one of which was previously oxidized in dry O<sub>2</sub> (NO-POA). Only the NO-annealed (NO-ox) sample exhibits a sharp-top main peak in the XANES spectrum. Conversely, the NO-POA sample exhibits an additional pre-edge peak. The peak shape and energy of the obtained and simulated spectra agree using SiO<sub>2</sub>/SiC interface models with N atoms inserted into the lattice. Consequently, the N-containing sites are probably substitutional C sites at the interface in the case of the NO-ox sample and an interstitial site in the SiC side in the case of the NO-POA sample. XAS can be used to distinguish between the N-containing sites at the SiO<sub>2</sub>/SiC interface by comparing the experimentally obtained and simulated spectra; apparently, simulation-aided XAS analysis can be used to improve the performance of high-power SiC-MOSFET devices.

### Acknowledgements

The authors are grateful to Dr Eiichi Kobayashi of SAGA-LS for his help with the XAS measurements and to the SiC power device development team members of Toyota Motor Corporation and DENSO Corporation for preparing the samples. The synchrotron radiation measurements were performed at BL12 of SAGA-LS with the approval of the Kyushu Synchrotron Light Research Center (Experimental Nos. 1706043G and 1801149G).

### References

Briggs, D. & Rivière, J. C. (1983). *Practical Surface Analysis*, edited by D. Briggs & M. P. Seah, p. 83. New York: John Wiley  
 Chang, Y. K., Hsieh, H. H., Pong, W. F., Tsai, M.-H., Lee, K. H., Dann, T. E., Chien, F. Z., Tseng, P. K., Tsang, K. L., Su, W. K., Chen, L. C., Wei, S. L., Chen, K. H., Bhusari, D. M. & Chen, Y. F. (1998). *Phys. Rev. B*, **58**, 9018–9024.  
 Chung, G. Y., Tin, C. C., Williams, J. R., McDonald, K., Di Ventra, M., Pantelides, S. T., Feldman, L. C. & Weller, R. A. (2000). *Appl. Phys. Lett.* **76**, 1713–1715.  
 Clark, S. J., Segall, M. D., Pickard, C. J., Hasnip, P. J., Probert, M. I. J., Refson, K. & Payne, M. C. (2005). *Z. Kristallogr.* **220**, 567.

Cook, P. L., Liu, X., Yang, W. & Himpsel, F. J. (2009). *J. Chem. Phys.* **131**, 194701.  
 Gao, S.-P., Pickard, C. J., Perlov, A. & Milman, V. (2009). *J. Phys. Condens. Matter*, **21**, 104203.  
 Hamada, K., Mikami, A., Naruoka, H. & Yamabe, K. (2017). *e-J. Surf. Sci. Nanotech.* **15**, 109–114.  
 Ikeno, H. & Mizoguchi, T. (2017). *Microscopy*, **66**, 305–327.  
 Isomura, N., Soejima, N., Iwasaki, S., Nomoto, T., Murai, T. & Kimoto, Y. (2015). *Appl. Surf. Sci.* **355**, 268–271.  
 Kaneyasu, T., Takabayashi, Y., Iwasaki, Y. & Koda, S. (2009). *Proceedings of the 12th International Conference on Accelerator and Large Experimental Physics Control Systems (ICALPECS 2009)*, 12–16 October 2009, Kobe, Japan, p. 307.  
 Kimoto, T. (2015). *Jpn. J. Appl. Phys.* **54**, 040103.  
 Kosugi, R., Umeda, T. & Sakuma, Y. (2011). *Appl. Phys. Lett.* **99**, 182111.  
 Li, H.-F., Dimitrijević, S., Harrison, H. B. & Sweatman, D. (1997). *Appl. Phys. Lett.* **70**, 2028–2030.  
 Mizoguchi, T., Matsunaga, K., Tochigi, E. & Ikuhara, Y. (2012). *Micron*, **43**, 37–42.  
 Mizoguchi, T., Tanaka, I., Gao, S.-P. & Pickard, C. J. (2009). *J. Phys. Condens. Matter*, **21**, 104204.  
 Mizoguchi, T., Tanaka, I., Yoshioka, S., Kunisu, M., Yamamoto, T. & Ching, W. Y. (2004). *Rhys. Rev. B* **70**, 045103.  
 Mizoguchi, T., Varela, M., Buban, J. P., Yamamoto, T. & Ikuhara, Y. (2008). *Phys. Rev. B*, **77**, 024504.  
 Norman, D. (1986). *J. Phys. C.: Solid State Phys.* **19**, 3273–3311.  
 Okumura, H. (2006). *Jpn. J. Appl. Phys.* **45**, 7565–7586.  
 Ono, T. & Saito, S. (2015). *Appl. Phys. Lett.* **106**, 081601.  
 Palgrave, R. G., Payne, D. J. & Egdell, R. G. (2009). *J. Mater. Chem.* **19**, 8418.  
 Perdew, J. P. (1985). *Phys. Rev. Lett.* **55**, 2370.  
 Ravel, B. & Newville, M. (2005). *J. Synchrotron Rad.* **12**, 537–541.  
 Shen, Z. J. & Omura, I. (2007). *Proc. IEEE*, **95**, 778–789.  
 Shirasawa, T., Hayashi, K., Mizuno, S., Tanaka, S., Nakatsuji, K., Komori, F. & Tochiwara, H. (2007). *Phys. Rev. Lett.* **98**, 136105.  
 Tanaka, I., Mizoguchi, T. & Yamamoto, T. (2005). *J. Am. Ceram. Soc.* **88**, 2013–2029.  
 Tanaka, T., Yamashita, H., Tsuchitani, R., Funabiki, T. & Yoshida, S. (1988). *J. Chem. Soc. Faraday Trans. 1*, **84**, 2987.  
 Xu, Y., Zhu, X., Lee, H. D., Xu, C., Shubeita, S. M., Ahyi, A. C., Sharma, Y., Williams, J. R., Lu, W., Ceesay, S., Tuttle, B. R., Wan, A., Pantelides, S. T., Gustafsson, T., Garfunkel, E. L. & Feldman, L. C. (2014). *J. Appl. Phys.* **115**, 033502.  
 Yoshioka, H., Nakamura, T. & Kimoto, T. (2012). *J. Appl. Phys.* **112**, 024520.